Chemosphere 280 (2021) 130647

Contents lists available at ScienceDirect

Chemosphere

journal homepage: www.elsevier.com/locate/chemosphere

Enhanced complexation of humic acids: Homogenization of protonated groups in the hybrid ozonation-coagulation process

Shiyi Hu [a], Xin Jin [a], Chao Yang [a], Yong Wang [a], Xinyue Xie [a], Shaohua Zhang [a], Pengkang Jin [a, b, *], Xiaochang C. Wang [a]

[a] School of Environmental and Municipal Engineering, Xi'an University of Architecture and Technology, Xi'an, Shaanxi Province, 710055, China
[b] School of Human Settlements and Civil Engineering, Xi'an Jiaotong University, Xi'an, Shaanxi Province, 710049, China

HIGHLIGHTS

- HOC process has a wider ozone dosage range than pre-ozonation-coagulation process.
- Ozone can react with hydrolysed Al species besides HA in the HOC process.
- Ozone homogenizes the protonated groups of HA and hydrolysed coagulant species.
- Simultaneous homogenization facilitates the binding between HA and coagulants.

GRAPHICAL ABSTRACT

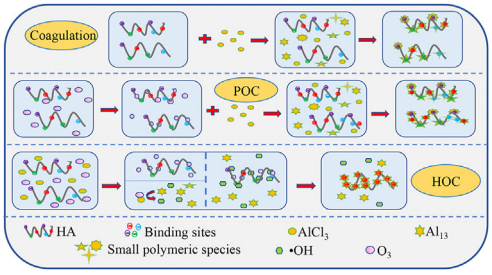

ARTICLE INFO

Article history:
Received 17 March 2021
Received in revised form
20 April 2021
Accepted 23 April 2021
Available online 25 April 2021

Handling Editor: E. Brillas

Keywords:
Hybrid ozonation-coagulation process
Organic functional groups
Coagulant hydrolysis
Complexation characteristics

ABSTRACT

In this study, we compared dissolved organic carbon (DOC) and UV_{254} removal efficiencies of the hybrid ozonation-coagulation (HOC) and pre-ozonation-coagulation (POC) processes for humic acid (HA) at pH 5 with $AlCl_3 \bullet 6H_2O$ as the coagulant. The DOC and UV_{254} removal efficiencies of the HOC process were higher than those of the POC process at ozone dosages less than 2.0 mg O_3 (mg DOC)$^{-1}$. The ozone dosage was optimized at 0.3 and 0.1 mg O_3 (mg DOC)$^{-1}$ for the HOC and POC processes, respectively, implying a more rigorous ozone dosage for the POC process. During the POC process, pre-ozonation was observed to increase the binding sites of HA (e.g., hydroxyl and carboxyl groups), improving the complexation of dissolved organic matter. For the HOC process, in addition to its role in the oxidation of organic matter, ozone also reacted with coagulants. The reaction between ozone and coagulants can facilitate the formation of Al_{13}. Moreover, the oxidation of •OH and ozone can increase the charge density of the HA binding sites, homogenizing the binding sites of HA and enhancing the complexation with Al_{13}.

1. Introduction

Coagulation can effectively remove particulate matter and colloid in water (Luo et al., 2014), yet effectively removing dissolved organic matter proves to be a complicated task (Stephenson and Duff, 1996; Jin et al., 2013). In order to improve the removal efficiency of dissolved organic matter in water, previous research has combined ozonation and coagulation to form the pre-ozonation-coagulation (POC) process (Yan et al., 2007; Li et al., 2009). Pre-ozonation can alter the structure of organic matter, increase the content of organic matter oxygen-containing functional groups (e.g., hydroxyl and carboxyl), and promote the complexation of

* Corresponding author. No. 13, Yanta Road, Beilin district, Xi'an, China.
E-mail address: pkjin@hotmail.com (P. Jin).

https://doi.org/10.1016/j.chemosphere.2021.130647
0045-6535/

organic matter and metal ions (Reckhow et al., 1986; Pei et al., 2007). During the pre-ozonation process, the oxidation of organic matter is achieved by molecular ozone oxidation.

However, ozone molecules can be selective in the oxidation of organic matter (Meunier et al., 2006). In particular, they favor reactions with electron-rich compounds (e.g., phenols, olefins, deprotonated amines and reduced sulfur groups) as a strategy to increase the number of oxygen-containing functional groups (Von Sonntag and Von Gunten, 2012; Hübner et al., 2015). The reaction rate of ozone molecules can be extremely slow for organic acids, aldehydes, ketones and several aromatic organic substances with low activity (Iglesias et al., 2003). In addition, the ozone dosage can affect the water quality of the effluent in the POC process (Farvardin and Collins, 1989). For small ozone dosages, ozone can strengthen the coagulation effect, while for more excessive dosages, ozone oxidation can affect the flocculating speed and stability of flocs during the subsequent coagulation process, increasing the effluent turbidity (Sam et al., 2010). Therefore, the ozone dosage must be strictly controlled during the POC process.

In order to overcome the limitations of the POC process, our previous studies proposed the hybrid ozonation-coagulation (HOC) process, involving the simultaneous occurrence of the ozonation and coagulation processes (Jin et al., 2017). During the HOC process, there are multiple reactions including coagulation, direct molecular ozone oxidation (MO reactions) and advanced oxidation processes (AOPs). AOPs include peroxone reactions (O_3/H_2O_2), •OH oxidation that from chain reactions during ozone decomposition (HO reactions) and the synergistic effects between ozone and the metal coagulants (SOC) (Jin et al., 2020a, 2020b). Similar to the POC process, the chain reaction during ozone decomposition in the HOC process is a result of the ozone reaction with OH^- in water, whereby the pH is lowered due to the consumption of OH^- in water. Moreover, organic matter is ozonated to produce a large number of intermediates that contain carboxyl groups (Xie et al., 2016). These carboxyl groups can also change the pH of the process through protonation, which consequently influences the coagulation performance. Ozone can also react with hydrolysed metal coagulants to produce •OH in the HOC process (Jin et al., 2017, 2019a).

•OH is a non-selective oxidant with a stronger oxidation ability compared to ozone (Nawrocki and Kasprzyk-Hordern, 2010). The •OH oxidation of organic matter typically occurs through H-abstraction, electron transfer and addition reactions, with the latter being the most common and fastest option (Von Sonntag and Von Gunten, 2012). •OH initially attacks the organic side chain to destroy its stable structure, and subsequently disconnects the bridge ring structure to form a single-ring product (Qi et al., 2009). Following this, •OH breaks the single-ring structure to form small molecules of aldehyde, ketone and acid products, and finally mineralizes to form CO_2 and H_2O (Qi et al., 2009; Fotiou et al., 2014). Furthermore, aromatic carbon is the preferred reaction site of •OH (Haag and Yao, 1992; Westerhoff et al., 1999). The production of •OH in Fenton oxidation has been reported to affect the coagulation removal of organic matter (Wu et al., 2010, 2011; Wang et al., 2021). More specifically, the coagulation removal of organic matter in Fenton reactions was observed to improve by increasing the hydrogen peroxide dosage within the range of 5–40 mM (Wu et al., 2010). Under these conditions, the organic matter oxidized by the Fenton process produces a large number of COO-containing intermediates, and the coagulation is able to effectively remove these contaminants (Han et al., 2020). In addition, the flocs produced in the Fenton process exhibit a larger specific surface area and a greater number of active sites compared to coagulation, thus supplying additional adsorption sites for the removal of organic matters (Italiano et al., 2018; Han et al., 2020). In contrast, the coagulation removal of organic matter was observed to decline rapidly as the hydrogen peroxide dosage increased continuously from 40 to 320 mM (Wu et al., 2010). This may be because the low molecular organics produced during the oxidation stage are less prone to coagulation, as Fenton oxidation and coagulation both have a preference for the removal of high molecular weight organics (Deng and Englehardt, 2006; Wu et al., 2010, 2011). Therefore, the effect of ozone and generated •OH on the coagulation during the HOC process requires further research.

The metal salt coagulants are hydrolyzed to form a variety of polyhydroxy polymerization hydrolysates in water, some of which can catalyze the decomposition of ozone to produce hydroxyl radicals (Ikhlaq et al., 2012). The surface charge, hydroxyl content and density, degree of polymerization, and ozone catalytic activity vary with the hydrolysis product type (Zhao et al., 2009). Ozone in aqueous solutions has been reported to interact with the surface hydroxyl groups on the catalysts via two basic attractive forces, namely electrostatic force or/and hydrogen bonding, forming $M-OH-O_3$ with an oxygen bridge connection (Beltran, 2003; Zhang et al., 2008). Moreover, a single O_2 molecule is released during this process through electron transfer and HO_2^- is generated on the surface of the coagulant (Zhang and Ma, 2008). The generation of $•HO_3^-$ and the adsorbed state of $•O_2^-$ attributed to the reaction between molecular ozone and HO_2^- can be converted into •OH through a chain reaction (Jin et al., 2017, 2019a, 2019b). The hydrolysis of the metal coagulant is a result of the deprotonation and hydroxyl bridging, and thus the complexation between the ozone and hydroxyl groups may influence the hydrolysis of the metal coagulant in the HOC process. However, studies on the effect of ozone on Al-based coagulant hydrolysis are lacking.

In the current study, we compared the removal efficiency of organic matter for commercial humic acid solutions via the HOC and the POC processes and $AlCl_3•6H_2O$ as the coagulant. Furthermore, in order to further clarify the organic matter removal mechanism of the HOC process, we analyzed the morphology and structure of the organic matter, as well as the coagulant hydrolysis form and the complexation characteristics between the organic matter and coagulant hydrolytic products under several processes.

2. Materials and methods

2.1. Materials and reagents

The stock HA solution was prepared by adding 1 g HA obtained from Sigma-Aldrich to 1 L 0.1 M NaOH solution, stirring for 12 h, the samples were filtered using a 0.45-μm membrane to remove particles. The stock HA solution was diluted with ionized water to reach the designated concentration (DOC = 5.5 mg L^{-1}).

2.2. Preparation of ozone stock solution

The ozone from a Sankang ozone generator (Model: SK-CFQ-5P, oxygen source, China) passed into deionized water adjusted to pH = 3 with phosphoric acid and aerated for 2 h at -1-4 °C. The prepared ozone water concentration was approximately 200 mg L^{-1} by Indigo Disulphonate Spectrophotometry (Yan et al., 2020).

2.3. Coagulation experiments

Coagulation tests were performed using jar-tests in six 500-mL beakers. Coagulation conditions involved rapid mix at 300 rpm (G = 670.4 s^{-1}) for 1 min, slow stirring at 60 rpm (G = 59.9 s^{-1}) for 30 min and a 30 min settling period. In the study, aluminum chloride ($AlCl_3•6H_2O$) was employed as coagulant, 1 mM Phosphate buffer was added into the solution to ensure the stability of pH and

0.1 M HNO_3 solutions were to adjust the pH of the solution.

2.4. POC experiments

The POC experiment required adding ozone stock solution to achieve the required dosage for oxidation, which slow stirring at 60 rpm ($G = 59.9\ s^{-1}$) for 15 min before coagulation. The following process was the same as coagulation experiments.

2.5. HOC experiments

The ozone stock solution was added at the beginning of the slow-mix step during coagulation. This allowed for the simultaneous occurrence of ozonation and coagulation.

2.6. Analytical methods

2.6.1. Dissolved organic carbon (DOC) analysis

DOC was measured using a Shimadzu $TOC_{V\text{-}CPH}$ analyzer. All samples were filtered through a 0.45-μm filter.

2.6.2. ^1H nuclear magnetic resonance (^1H NMR) spectroscopy analysis

Each sample used for ^1H NMR analysis was pre-treated via solid phase extraction (SPE) and then dissolved into D_2O (Jin et al., 2018). ^1H NMR spectra were obtained with a Bruker Advance 400 MHz NMR spectrometer equipped with a 5-mm resonance broadband observe probe.

2.6.3. X-ray photoelectron spectroscopy (XPS) analysis

Following treatment, the flocs were separated from the solution by centrifugation and lyophilized in order to perform the XPS analysis. In addition, after adjusting the stock HA solution to pH 5, the lyophilized HA samples were analyzed as pre-treatment samples. The XPS spectra were obtained using a K-Alpha X-ray photoelectron spectrometer (Thermo Fisher Scientific, UK). The binding energy within 100–1000 eV and the core-level characteristic peaks for C 1s and Al 2p.

2.6.4. ^{27}Al nuclear magnetic resonance (^{27}Al-NMR) analysis

Solid ^{27}Al-NMR was tested on the Advance 400 Bruker pulsed Fourier nuclear magnetic resonance instrument. The lyophilized samples were loaded into 4 mm NMR tubes and measured at 78.2 MHz and 328 K, with pulse and spectrum widths of 0.3 μs and 60 Hz, respectively (Song et al., 2019b).

2.6.5. Solid-state ^{13}C nuclear magnetic resonance (^{13}C NMR) spectroscopy analysis

Solid ^{13}C NMR was collected following the method of ^{27}Al-NMR, with measurements at 100.63 MHz and 6.0 kHZ, and sample cycle time and the sampling time of 1.2 s and 42 ms, respectively.

2.6.6. Fourier transform infrared spectroscopy (FT-IR) analysis

The samples were obtained via a mixture of 1 mg flocs and 99 mg KBr. Spectra we collected using an FT-IR spectrometer (Nicolet 6700, Thermo Fisher Scientific,UK) with the range of 3950 to 450 cm^{-1} (Jin et al., 2020b).

2.6.7. Excitation-emission matrix (EEM) analysis

Three-dimensional fluorescence spectra in the form of EEM plots were recorded using an F-7000 fluorescence spectrophotometer (Hitachi, Japan). The EEM spectra of the samples were scanned over an excitation range of 220–480 nm with 5 nm intervals and an emission range of 280–550 nm with 2 nm intervals, the excitation and emission slit widths were 5 nm (Jin et al., 2016). The scan rate was set to 12,000 nm min^{-1}.

3. Results and discussions

3.1. Removal performance

Fig. 1 presents the DOC and UV_{254} removal efficiencies of the HOC and POC processes for HA at pH 5 and 2.75 mg Al L^{-1}. For ozone dosages less than 0.7 mg O_3 (mg DOC)$^{-1}$, the UV_{254} and DOC removal efficiencies of the POC process exceeded those of the coagulation process (ozone dosage = 0 mg O_3 (mg DOC)$^{-1}$). However, the UV_{254} and DOC removal efficiencies of the POC process were lower than those in the coagulation process when the ozone dosages was more than 0.7 mg O_3 (mg DOC)$^{-1}$. This can be attributed to the HA over-oxidation, which transforms organic matter with high molecular weight into low molecular weight organic matter that cannot be effectively removed by the subsequent coagulation (Chandrakanth and Amy, 1998; Bose and Reckhow, 2007).

The ozone dosage exhibited a wider range in the HOC process compared to the POC process. For ozone dosages less than 2.0 mg O_3 (mg DOC)$^{-1}$, the UV_{254} and DOC removal efficiencies of the HOC process were higher than those of the coagulation process. At the same ozone dosages, the HOC process also exhibited superior DOC and UV_{254} removal efficiencies compared to the POC process. This indicates the mutual promotion of ozonation and coagulation during the HOC process. Our previous study also implied the ability of the Al-based coagulant to catalyze the decomposition of ozone,

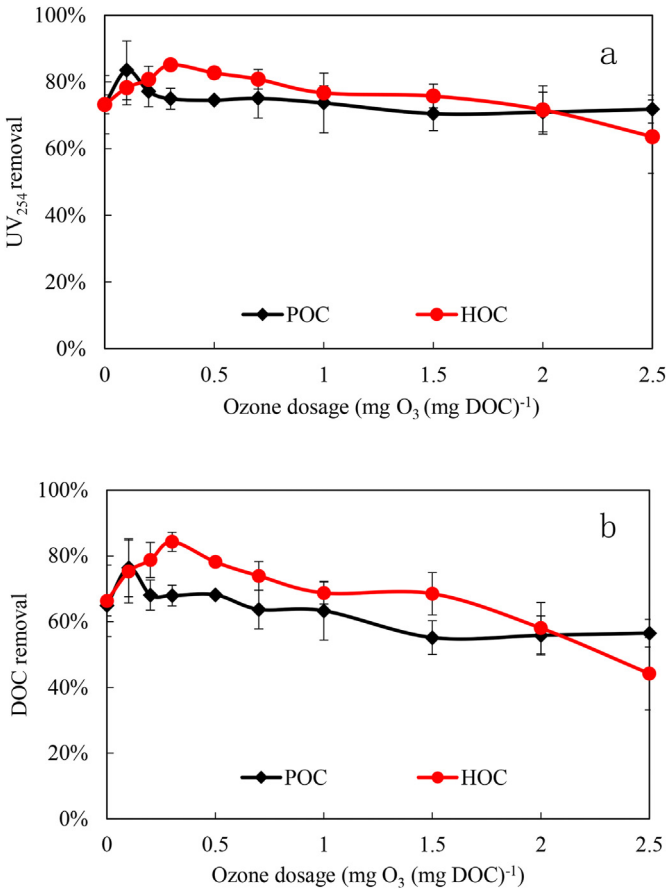

Fig. 1. DOC and UV_{254} removal performance of the HOC and POC processes at pH = 5 and 2.75 mg Al L^{-1}. a: UV_{254}, b: DOC.

resulting in the generation of hydroxyl radicals in the Al–HOC process and subsequently improving the dissolved organic matter removal performance (Jin et al., 2017). The DOC and UV_{254} removal efficiencies peaked at the ozone dosage was 0.3 and 0.1 mg O_3 (mg DOC)$^{-1}$ for the HOC and POC processes, respectively.

For ozone dosages exceeding 0.1 mg O_3 (mg DOC)$^{-1}$ during the POC process, the humic acid solution was over-oxidized and the organic matter removal efficiency was reduced. Moreover, during the HOC process, the organic matter removal efficiency began to deteriorate for ozone dosages greater than 0.3 mg O_3 (mg DOC)$^{-1}$. This indicates the absence of the over-oxidation of organic matter at this ozone dosage levels in the HOC process, with a portion of the ozone reacting with the coagulant to produce •OH, thus increasing the ozone consumption (Jin et al., 2017, 2019b). Moreover, •OH also demonstrates the ability to mineralize small organic matter molecules in water.

3.2. Homogenization of organic protonation in the HOC and POC processes

3.2.1. ^{1}H NMR analysis

In order to clarify the modification of organic matter protonic groups resulting from the HOC and POC processes, ^{1}H NMR spectra were analyzed to reveal the structural characteristics of the organic matter. Fig. S1 and S2 depict the organic matter ^{1}H NMR spectra before and after the POC and HOC treatments at the ozone dosages of 0.1, 0.3, 1.0 mg O_3 (mg DOC)$^{-1}$. The HA ^{1}H NMR spectra can be divided into five resonance ranges: (1) aliphatic (HC–C–C-): chemical shift range 0.0–1.9 ppm; (2) acetate analogue and carboxyl-rich alicyclic material (CRAM) (H–C–C–O): chemical shift range 1.9–3.1 ppm; (3) carbohydrate-like and methoxy (HCO): chemical shift range 3.1–4.9 ppm (4.7 ppm resonance corresponds to a chemical shift of D_2O); (4) olefin (HC= C, HCO_2): chemical shift range 5.3–7.0 ppm; and (5) aromatic (H_{ar}): chemical shift range 7.0–9.0 ppm (Cortés-Francisco et al., 2014). The Bruker software was used to calculate the ^{1}H NMR spectrum areas (Jin et al., 2018). The relative contents of the protonated groups containing the HA residual organic matter under the different processes was estimated via the Fig. 2a spectrum areas (Jin et al., 2018).

The hydrocarbon environment of the residual organic matter within the HA solution varied greatly across the processes. The raw water of the HA solution exhibited the highest aromatic proton content (53.64%). Following coagulation, the proportion of olefin in the remaining organic matter from the humic acid solution was observed to increase. The proportions of carbohydrate-like functional groups and methoxy were maintained constant, with the proportion of the remaining functional groups decreased. This indicates the selectiveness of the complexation process between $AlCl_3$•$6H_2O$ and the organic compounds during the coagulation process. Numerous studies have proven the complexation between organic functional groups and aluminum-salt coagulants to be selective (Kim and Yu, 2005; Zhang et al., 2012; Jin et al., 2018).

Humic acids contain a large number of functional groups, including carboxyl groups, phenolic hydroxyl groups, carbonyl groups, amines, amino compounds and esters (Bigalke et al., 2010). These functional groups exhibit distinct affinities with metal ions (Provenzano et al., 2004; Tipping, 2005). Functional groups with the ability to release protons and bind with metal ions are denoted as binding sites (Tipping et al., 1988; Pinheiro et al., 2000). The principle binding sites of HA are the hydroxyl and carboxyl groups (Iglesias et al., 2003; Kostic et al., 2011), and are thus easy to complex with $AlCl_3$•$6H_2O$ (Iglesias et al., 2003). Moreover, Jin et al., (2018) demonstrated the selectivity of the binding of aluminum-salt coagulants to organic compounds in humic acid solutions (Jin et al., 2018).

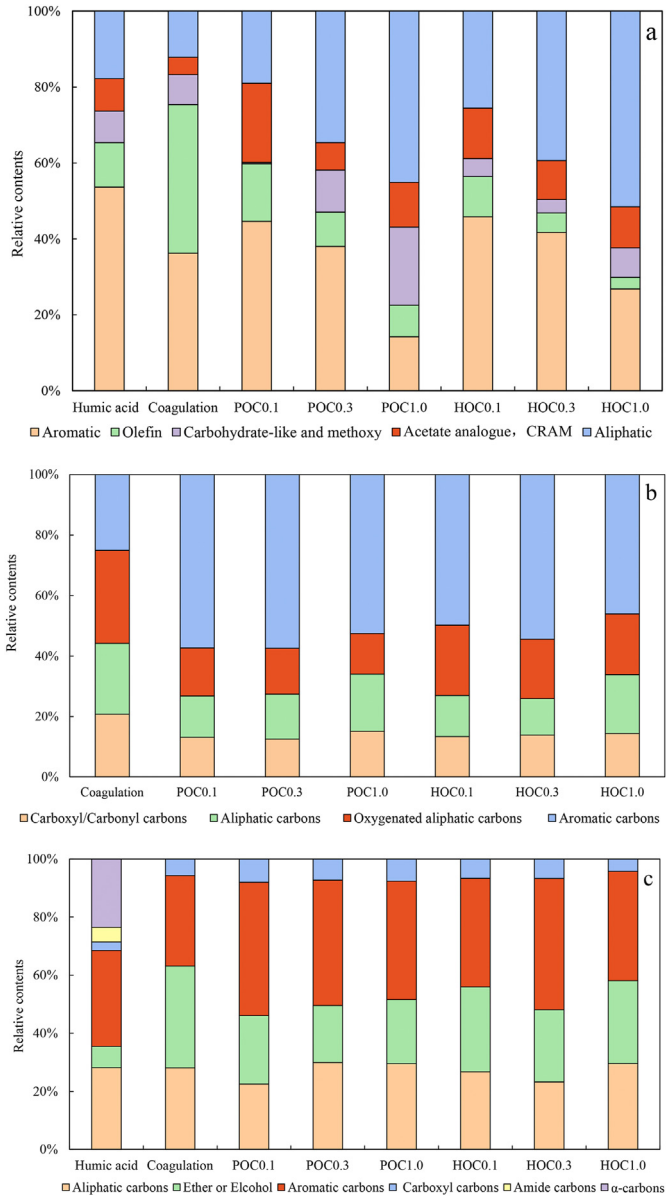

Fig. 2. The structures of organic matters of HA during different processes. a: residual organic matters during different processes by ^{1}H NMR, b: removed organic matters during different processes by ^{13}C NMR, c: removed organic matters during different processes by C 1s XPS.

The total proportion of aromatic and olefin compounds exhibited a decline in the HOC and POC processes compared with coagulation, while the opposite was true for the proportion of aliphatic organic matter. This indicates the ability of ozone to alter the structure of organic matter. The results reveal that the aromatic substances, olefin and other functional groups with unsaturated bonds were oxidized into aliphatic compounds by ozone during the HOC and POC processes, generating hydroxyl radicals. At low ozone dosages (0.1 mg O_3 (mg DOC)$^{-1}$) during the POC and HOC processes, the proportion of olefin was reduced compared to coagulation, while that of aromatic compounds increased. This reveals that olefin was oxidized preferentially. In addition, the relative contents of aliphatic increased with the ozone dosage, while the opposite was observed for the aromatics and olefin ratios. The

proportion of olefin and oxygen-containing functional groups in the POC process exceeded that of the HOC process. This is associated with the less selective and stronger oxidation ability of the •OH generated in the HOC process.

3.2.2. Solid ^{13}C NMR analysis

Fig. S3 and S4 depict the ^{13}C NMR spectra of HA flocs during the POC and HOC processes at the ozone dosages of 0, 0.1, 0.3, 1.0 mg O_3 (mg DOC)$^{-1}$. The HA spectra of both processes exhibit a similar general trend, with distinguishable peaks at approximately 28, 62, 75, 130, 155 and 170 ppm. The peak at 28 ppm corresponds to methyl and methylene carbons while the peaks at 62 and 75 ppm are attributed to methoxy and ring-ether functions, respectively (Monteil-Rivera et al., 2000). The strong intensity within the region of 100–160 ppm indicates the presence of a large number of aromatic carbons, with the peak at 130 ppm corresponding to C- and H-substituted carbon, while the 155 ppm peak is linked to O- and N-substituted carbon (Kögel-Knabner, 1997; Kölbl and Kögel-Knabner, 2004; Mao et al., 2008). The peak at 170 ppm is assigned to carboxyl, amide and ester carbons (Monteil-Rivera et al., 2000).

The spectra were subsequently divided into four different regions corresponding to the following dominant carbon types: aliphatic carbons (0–45 ppm); oxygenated aliphatic carbons (45–110 ppm); aromatic carbons (110–160 ppm); and carboxyl/carbonyl carbons (160–220 ppm) (Xiaoli et al., 2008). The values and peak areas of the chemical shift ranges were maximized within 110–150 ppm. This was attributed to the HA skeleton, which is composed of aromatic rings across different connections. Fig. 2b presents the ^{13}C NMR spectral area, determined using the software provided by Bruker.

The proportion of aromatic carbons in the HA flocs after the POC and HOC processes surpassed that of coagulation. Previous studies indicate the formation of the HA skeleton from the aromatic structure (Schnitzer and Khan, 1972; Schulten and Schnitzer, 1993). The relative contents of aliphatic carbons in the flocs increased with ozone dosage during both the HOC and POC processes. This is consistent with the ^{1}H NMR result. Aromatic compounds containing electron-giving groups (such as phenols and anilines) are prone to react with ozone molecules to form ortho-hydroxyl or para-hydroxyl compounds. Such compounds are more likely to be subject to further ozonation, generating ketones or opening aromatic rings to form aliphatic compounds with carbonyl and carboxyl groups (Camel and Bermond, 1998).

The sum of aliphatic and oxygenated aliphatic carbons in the HOC process surpassed that of the POC process at the same ozone dosage. This indicates the stronger removal effect of aliphatic carbons in the HOC process. The mechanisms underlying this result are two-fold: i) the non-selective oxidative modification of aliphatic carbons via the hydroxyl radical improved the cohesiveness (Meunier et al., 2006; Hübner et al., 2015); and ii) the interaction between ozone and the coagulant enhanced the coagulation ability of the coagulant (Xie et al., 2016).

3.2.3. C 1s XPS analysis

The high-resolution XPS spectra of the carbon element C 1s in the treated HA flocs and performed are shown in Fig. S5. Six overlapping peaks were observed in the C 1s spectra of HA at 289.19, 288.2, 286.8, 285.87, 285.2 and 284.58 eV, attributed to carboxyl carbons (C̲OO), amide carbons (C̲ON), ether or alcohol (C̲–O), α-carbons (C̲–CO), aliphatic carbons (C̲–C/C̲–H) and aromatic carbon (C̲–C/C̲–H), respectively (Monteil-Rivera et al., 2000; Jin et al., 2018). However, only four characteristic peaks (attributed to aromatic carbons, aliphatic carbons, ether or alcohol and carboxyl group) appeared in the C 1s floc spectra treated by different processes.

Fig. 2c presents the relative concentration of each component estimated by fitting the C 1s spectra of HA with the simulated C 1s spectra of the components. Under acidic conditions, the complexation between the hydrolysed species of $AlCl_3$•$6H_2O$ and organic matter was selective (Song et al., 2019b). This reduced the functional group types in the flocs following each process. The post-HOC and POC aromatic carbon proportion in the flocs was greater than that of coagulation, indicating the ability of ozone oxidation to promote the removal of humic acid. The ^{13}C NMR and C 1s XPS analysis results reveal that at 0.3 mg O_3 (mg DOC)$^{-1}$, the aromatic carbon content in the HOC process was higher than at 0.1 mg O_3 (mg DOC)$^{-1}$. This is consistent with the TOC removal efficiency, indicating that at 0.3 mg O_3 (mg DOC)$^{-1}$, the organic matter modified by ozone can better complex with metal coagulants and enhance the removal of HA.

3.2.4. FT-IR analysis

Fig. 3 presents the FT-IR spectra of the HA flocs before and after the different treatments. The raw humic acid solution exhibited multiple peaks around 800, 1100, 1380, 1630, 2500 and 3450 cm^{-1}, with the strongest peak intensities observed at 1100, 1380, 1630 and 3450 cm^{-1}. Table S1 reports the attribution of the infrared spectrum characteristic peaks (Miikki et al., 1997; Francioso et al., 2002; Amir et al., 2010). The FT-IR spectra of the HA flocs exhibited similar trends across treatments, indicating the similarity of organic functional group structures removed by the different processes.

However, under the same process, the FT-IR spectra varied with the ozone dosage. There were differences in the shape and intensity of the 3450, 1630 and 1100 cm^{-1} peaks from the HA flocs treated by coagulation and the raw HA The increased intensity of the 3450 and 1100 cm^{-1} peaks can be attributed to the –OH vibration of the hydroxyl groups, while the 1630 cm^{-1} peak is linked to by the water molecules attached to the surface of the coagulants surface (Li et al., 2004; Huang et al., 2019).

The intensity of the 1100 and 1630 cm^{-1} peaks in the POC and HOC processes were stronger than those of coagulation. This indicates that the oxygen-containing functional groups increased on aromatic rings of the humic acid flocs treated by the POC and HOC processes. Ozone molecules are selective for the oxidation of organic matter and also have a limited oxidation capacity. Therefore, during the POC process, the 1100 and 1630 cm^{-1} peak intensities did not increase significantly with the ozone dosage. During the HOC process, the intensities of the 1100, 1630 and 3450 cm^{-1} peaks initially increased and subsequently decreased with the increasing ozone dosage. This is consistent with the removal efficiency of organic matter.

Under the same ozone dosage, the 1100, 1630 and 3450 cm^{-1} peak intensities of the HOC process exceeded those of the POC process, indicating that the amount of oxygen-containing functional groups on the aromatic rings of the flocs treated by the former were higher than those of the latter. This is attributed to the oxidation of organic matter by ozone and reactive oxygen species (ROS), which tends to homogenize the functional groups of organic matter and increases the number of oxygen-containing functional groups (e.g., hydroxyl and carboxyl groups) in HA.

3.3. Hydrolyzed species and coagulation behavior of $AlCl_3$•$6H_2O$ in the HOC and POC processes

3.3.1. ^{27}Al-NMR analysis

Fig. 4 presents the ^{27}Al-NMR spectra of the flocs produced under the different processes. Two distinctive resonances can be observed

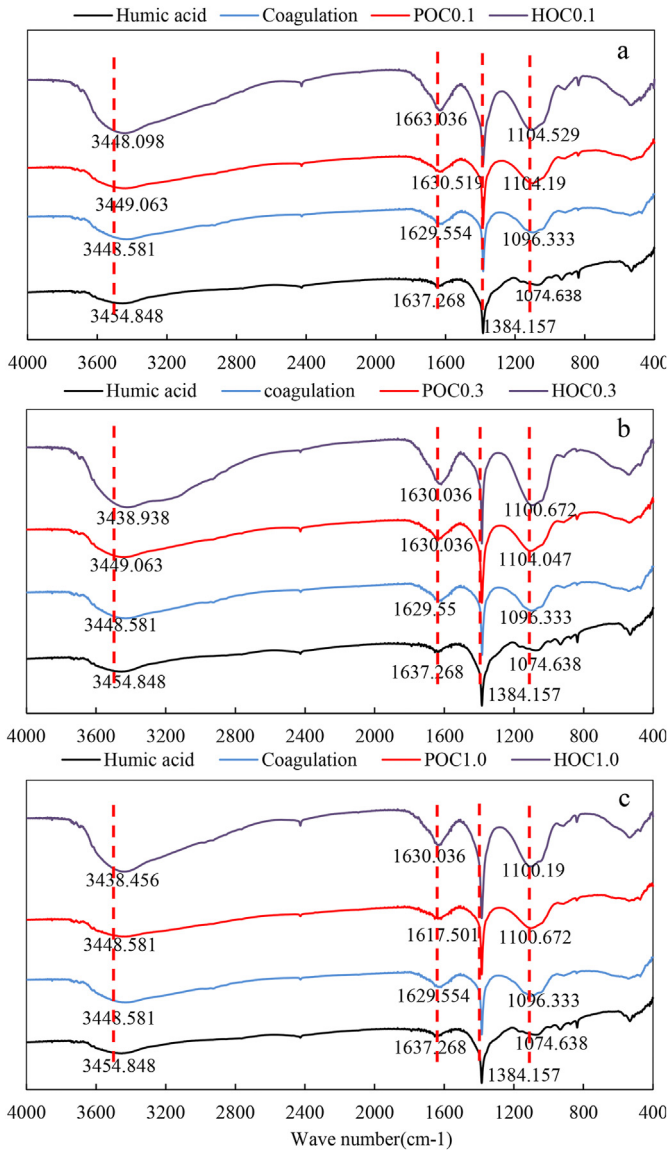

Fig. 3. FT-IR spectra of HA flocs at different ozone dosages. a: 0.1 mg O_3 (mg DOC)$^{-1}$, b: 0.3 mg O_3 (mg DOC)$^{-1}$, c: 1.0 mg O_3 (mg DOC)$^{-1}$..

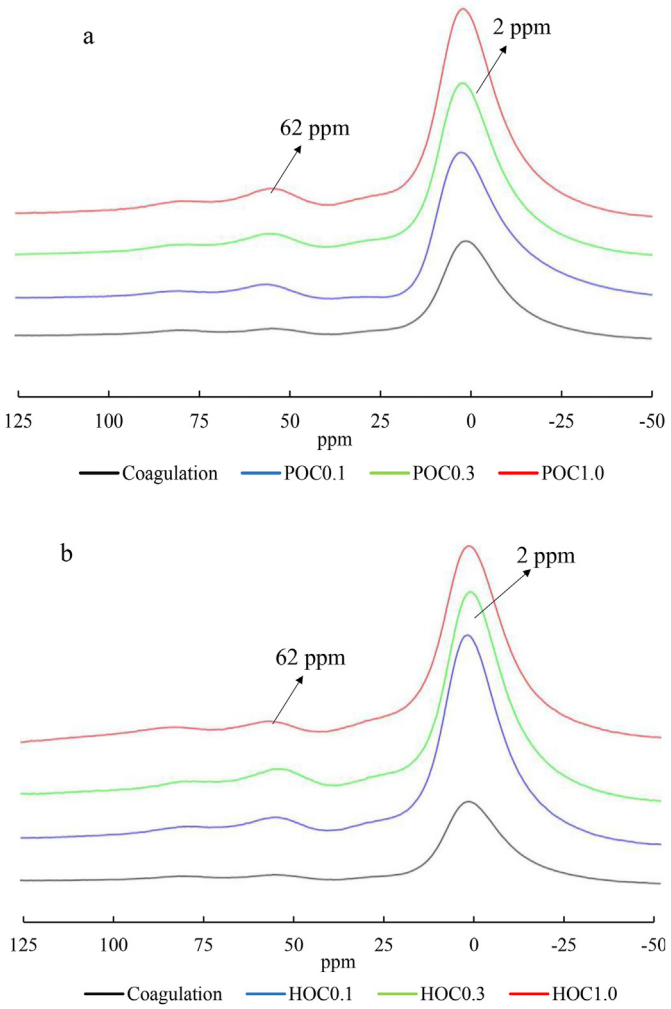

Fig. 4. ^{27}Al-NMR spectra of HA flocs treated by different processes. a: POC processes, b: HOC processes.

in the ^{27}Al-NMR spectra, with chemical shifts of the two peaks equal to 2 and 62 ppm, respectively. The strongest asymmetric resonance peak with the 2 ppm chemical shift corresponds to octahedral coordinated aluminum, and more specifically, the 'free' Al dimers or complexed Al monomers and dimers (Zhao et al., 2009; Song et al., 2019b). The weaker resonance peaks at 62 ppm represent the central tetrahedral aluminum morphology of Al_{13}, where the distinct formation and aging conditions of Al_{13} typically result in peaks within the 61–64 ppm range (Liu et al., 2009).

The Al_{13} contained in the hydrolyzed species of the aluminum salt coagulant is a polyhydroxy complex composed of 12 six-coordinate octahedral aluminum atoms surrounding a four-coordinate tetrahedral aluminum atom with hydroxyl bridges (Hiradate and Yamaguchi, 2003). The four-coordinated aluminum atom in the symmetrical center of Al_{13} produces a resonance peak at the chemical shift of 62 ppm in the ^{27}Al-NMR spectra (Jin et al., 2019a). However, the six-coordinated octahedral aluminum atom in the asymmetric environment is not able to generate resonance peaks in the NMR spectrum. Therefore, following the quantitative calculations, the actual content of Al_{13} in the flocs was 13 times that of the aluminum content corresponding to the 62 ppm resonance peak (Hiradate and Yamaguchi, 2003). Despite the low peak response of the 62 ppm chemical shift and the key role of Al_{13} as the aluminum form in the flocs, it still exerted the greatest influence on the removal of humic acid.

Fig. 4 demonstrates Al_{13} polymer, monomeric and dimeric aluminum to be the Al species produced by different processes in the flocs. This indicates that the humic acid contained in the water was removed by complexation with several hydrolysis products of $AlCl_3 \bullet 6H_2O$ under the different processes.

3.3.2. Al 2p XPS analysis

Fig. S6 presents the Al 2p spectra of the XPS for the different process. Two overlapping bands are observed in the humic acid flocs treated by different processes, associated with two different Al 2p transitions. The binding energy of the two overlapping bands are 72 and 74 eV, corresponding to tetrahedral aluminum and octahedral aluminum respectively (Ernst et al., 2004; Duong et al., 2005). Tetrahedral Al and octahedral Al have previously been associated with the AlO_4 unit structure and the AlO_6 structure, respectively (Suresh et al., 2012).

Fig. 5 presents the relative content of various aluminums species contained in the humic acid flocs under the different treatments.

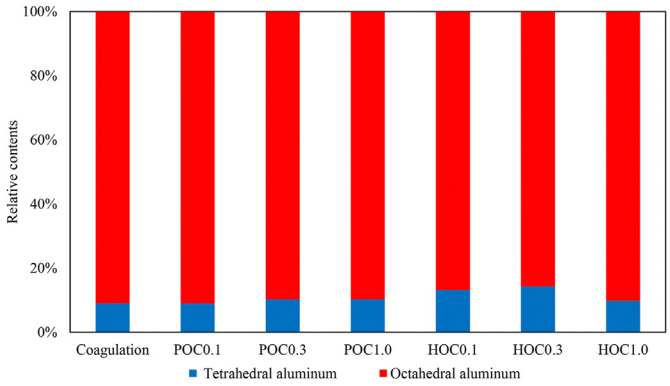

Fig. 5. The relative contents of various aluminum species in contained in the HA flocs under the different treatments.

The Al (III) Tet/Al (III) Oct ratio of the humic acid flocs generated by coagulation was determined as 1:10, suggesting the occurrence of a large amount of tetrahedral aluminum on the floc surface. Theoretically, the Al (III) Tet/Al (III) Oct ratio in Al_{13} molecules should be approximately equal to 1:12 (Hiradate and Yamaguchi, 2003). This proves that only a small to medium number of tetrahedral aluminums existed in the form of Al_{13} in flocs. The relative contents of tetrahedral aluminum in the flocs formed by the POC and coagulation processes exhibited similar trends, while the tetrahedral aluminum contents formed by the HOC process was higher than that of the POC process. Furthermore, the removal efficiency of organic matter was related to the aluminum form. The central aluminum form of Al_{13} was tetrahedral aluminum, while Al_{13} was also the dominant hydrolysis form $AlCl_3 \bullet 6H_2O$ during coagulation (Lin et al., 2008, 2014). Therefore, the removal efficiency of organic matter was superior in the HOC process compared to the POC process.

3.4. Complexation between $AlCl_3 \bullet 6H_2O$ and HA in the HOC and POC processes

Fig. 6 depicts the EEM spectra of the commercial humic acid solution before and after the different treatments. The EEM spectra exhibited a single peak, which corresponds to the humic-like substances.

The intensity of EEM spectra implied the content of benzene rings and conjugated unsaturated bonds in organic matter (White et al., 2003). Following coagulation, the fluorescence intensity in the solution was slightly stronger than that in the humic acid stock solution. However, the DOC levels in the HA solution were observed to decrease after coagulation, indicating the impact of the complexation between the hydrolysed products of the coagulant and the dissolved organic matters on the fluorescence intensity of organic matter (Provenzano et al., 2004). The rigid structures in the molecules have been reported to enhance the fluorescence intensity of organic matter (Oliver et al., 1983; Provenzano et al., 2004). If HA forms complexes with metal salts, the fluorescence would be either enhanced or quenched (Sharpless and Mcgown, 1999; Elkins and Nelson, 2002). Moreover, humic acid complexed with the hydrolysed products of $AlCl_3 \bullet 6H_2O$ to form a complex, which enhanced the rigidity structures of humic acid. This consequently increased the fluorescence intensity of the HA solution following coagulation.

During the POC process, the fluorescence intensity decreased with increasing ozone dosage. This is associated with the conjugated unsaturated structures in humic acid being oxidized during the pre-ozonation process. The conjugated unsaturated structures in humic acid were oxidized at a greater rate with increasing ozone dosage, thus weakening the fluorescence intensity.

At the ozone dosages of 0.1 and 0.3 mg O_3 (mg DOC)$^{-1}$, the fluorescence intensities were not observed to decrease during the HOC process. In contrast, when the ozone dosage was 1.0 mg O_3 (mg DOC)$^{-1}$, the fluorescence intensity in the treated humic acid was weakened, with the HOC process resulting in a greater fluorescence intensity compared to the POC process. However, the removal efficiency of organic matter in the HOC process was stronger than that in the POC process. This may be attributed to the enhanced complexing ability of organic matter and hydrolysed coagulant hydrolysates species, resulting in the enhanced structural rigidity of organic matter and the subsequent variations in the fluorescence intensity of organic matter (Sharpless and Mcgown, 1999; Elkins and Nelson, 2002). When the dosage of ozone increased to 1.0 mg O_3 (mg DOC)$^{-1}$, part of the organic matter was completely or excessively oxidized, thus affecting the complexation between the coagulant and organic matter. This reduced the fluorescence intensity and organic matter removal efficiency.

3.5. Proposed mechanism

Based on the comparison between the POC and HOC processes, we proposed a mechanism for the ozonation effect on the complexation properties of the protonated groups containing organic matter as Fig. 7. Under acidic conditions, the removal of organic matter typically occurs through the complexation between different in situ hydrolyzed aluminum species and the corresponding binding sites on the humic acid during coagulation (Song et al., 2019a). During the POC process, ozone only acts on organic pollutants and is able to change the structure of organic matter and increase the HA binding sites (e.g., hydroxyl and carboxyl groups) (Pei et al., 2007; Kostic et al., 2011). This enhances the complexation between organic matters andthe coagulant, thus improving the removal rate of organic matters. Moreover, during the HOC process, ozone molecules increase the HA binding sites and also undergo multiple catalytic oxidation reactions, for example peroxone reactions (O_3/H_2O_2) and the synergistic effects between ozone and the metal coagulants (SOC), enhancing the •OH content in the process (Jin et al., 2020b). Note that •OH is a non-selective oxidant, and can assist in eliminating ozone-refractory pollutants (Nawrocki and Kasprzyk-Hordern, 2010; Wang and Chen, 2020).

In addition, ozone combines with the surface hydroxyl groups of the coagulant hydrolysed products in the HOC process, converting most $AlCl_3 \bullet 6H_2O$ hydrolysed species to Al_{13}. Our previous study demonstrated the coagulation efficiency of HA by Al_{13} to be worse than that of $AlCl_3 \bullet 6H_2O$ at acidic conditions (Song et al., 2019a). Homogenized Al_{13} with high positive charges was not able to effectively complex the negative binding sites of HA with lower charge densities in the coagulation process, consequently lowering the organic matters removal efficiency (Song et al., 2019a). However, in the current study, the removal efficiency of organic matter in the HOC process was superior to that of the coagulation and POC processes, despite the hydrolysed aluminum species present in the form of Al_{13} in the HOC process. This may be attributed to the increase in charge density of the HA binding sites due to ozone and

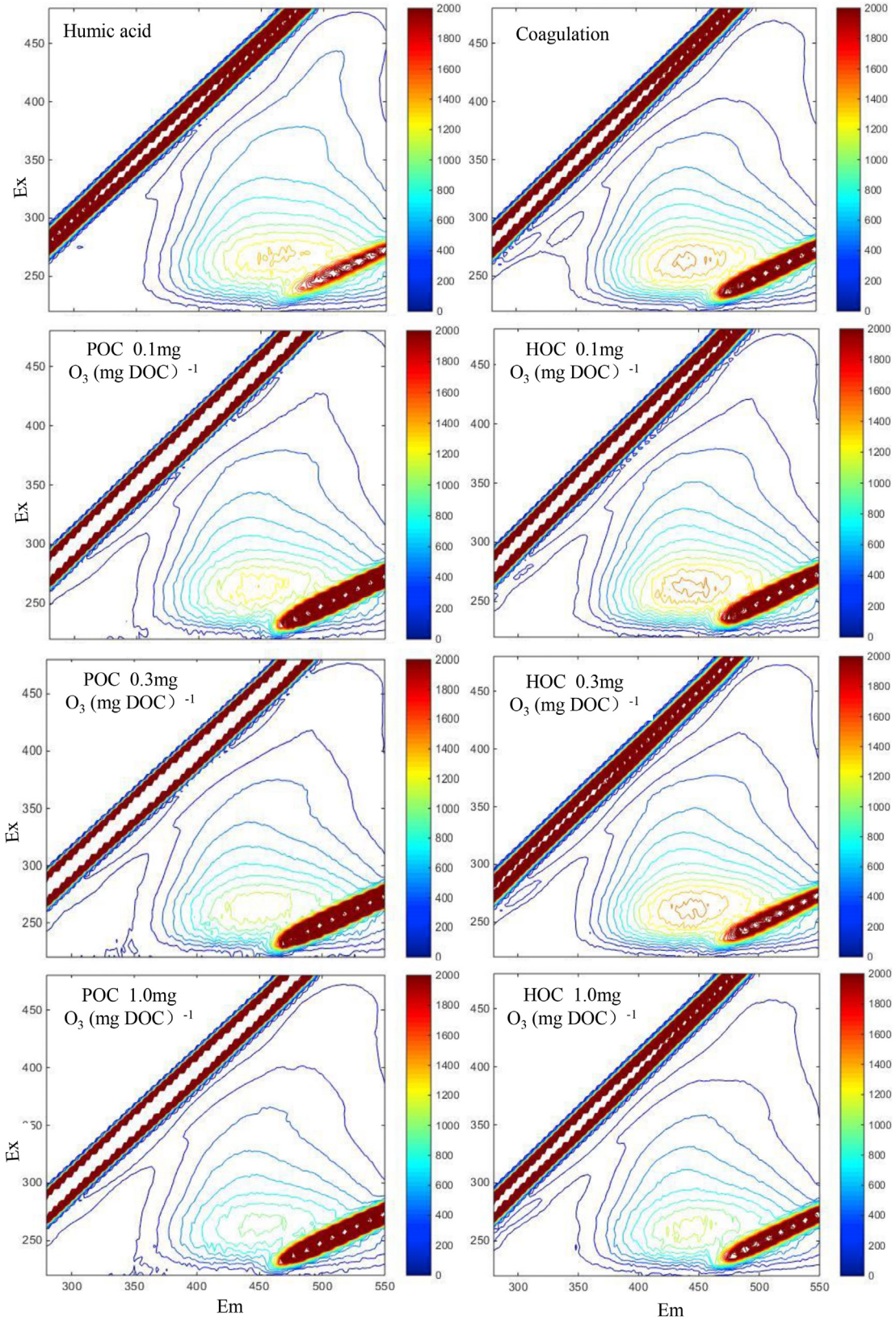

Fig. 6. The EEM spectra of HA solution before and after treated by different processes.

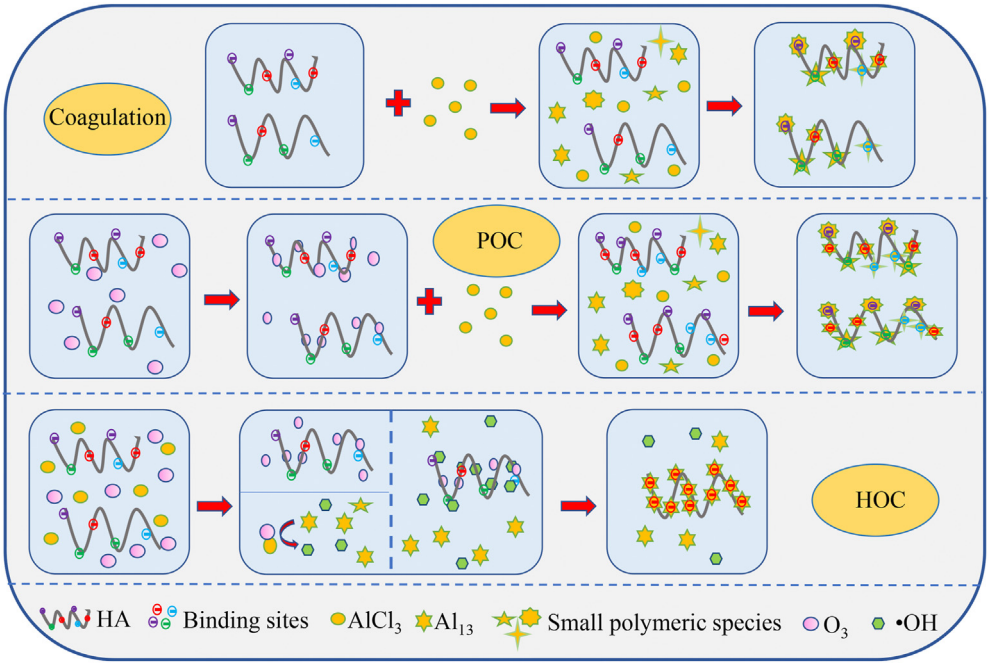

Fig. 7. The mechanism of organic matter removal during the POC and HOC processes.

•OH oxidation in the HOC system (Önnby et al., 2018; Walpen et al., 2020), thus homogenizing the binding sites and facilitating the binding with coagulant.

4. Conclusions

Under the same ozone dosage, the organic matter removal efficiency of the HOC process exceeds that of the POC process for HA at pH = 5. The optimal ozone dosage was identified as 0.1 and 0.3 mg O_3/mg TOC for the POC and HOC processes, respectively. The HOC process exhibits a wider range of ozone dosage (<2.0 mg O_3 (mg DOC)$^{-1}$) than the POC process (<0.7 mg O_3 (mg DOC)$^{-1}$). Moreover, the ozone and (ROS) in the HOC process were able to oxidize organic matter more effectively compared to the POC process, resulting in the homogenization of the organic matter structures. The Al 2p XPS and ^{27}Al NMR analysis revealed a greater amount of tetrahedron aluminum to be present in the HOC process, proving that ozone altered the hydrolysed species of $AlCl_3$•$6H_2O$. Furthermore, the ozone oxidation of organic matter and the $AlCl_3$•$6H_2O$ coagulant during the HOC process enhanced the complexation between them, increasing the removal efficiency of organic matter.

Declaration of competing interest

The authors declare that they have no known competing financial interests or personal relationships that could have appeared to influence the work reported in this paper.

Acknowledgements

This work was supported by the National Natural Science Foundation of China (No. 52070151, 51708443), the National Key R&D Program of China (No. 2019YFB2103003), the Key Research and Development Project of Shaanxi Province (2019ZDLSF05-03), the New Style Think Tank of Shaanxi Universities and the Scientific Research Program of Shaanxi Provincial Education Department (No. 18JS057).

Appendix A. Supplementary data

Supplementary data to this article can be found online at https://doi.org/10.1016/j.chemosphere.2021.130647.

Credit author statement

Shiyi Hu: Investigation, Formal analysis, Data curation, Roles/Writing - original draft. Xin Jin: Writing – review & editing. Chao Yang: Methodology. Yong Wang: Software, Xinyue Xie: Visualization. Shaohua Zhang: Resources, Pengkang Jin: Conceptualization, Supervision. Xiaochang C. Wang: Conceptualization

References

Amir, S., Jouraiphy, A., Meddich, A., El Gharous, M., Winterton, P., Hafidi, M., 2010. Structural study of humic acids during composting of activated sludge-green waste: elemental analysis, FTIR and 13C NMR. J. Hazard Mater. 177, 524–529.
Beltran, F.J., 2003. Ozone Reaction Kinetics for Water and Wastewater Systems, vol. 128. crc Press (2-3), 295-295.
Bigalke, M., Weyer, S., Wilcke, W., 2010. Copper isotope fractionation during complexation with insolubilized humic acid. Environ. Sci. Technol. 44, 5496–5502.
Bose, P., Reckhow, D.A., 2007. The effect of ozonation on natural organic matter removal by alum coagulation. Water Res. 41, 1516–1524.
Camel, V., Bermond, A., 1998. The use of ozone and associated oxidation processes in drinking water treatment. Water Res. 32, 3208–3222.
Chandrakanth, M.S., Amy, G.L., 1998. Effects of NOM source variations and calcium complexation capacity on ozone-induced particle destabilization. Water Res. 32, 115–124.
Cortés-Francisco, N., Harir, M., Lucio, M., Ribera, G., Martínez-Lladó, X., Rovira, M., Schmitt-Kopplin, P., Hertkorn, N., Caixach, J., 2014. High-field FT-ICR mass spectrometry and NMR spectroscopy to characterize DOM removal through a nanofiltration pilot plant. Water Res. 67, 154–165.
Deng, Y., Englehardt, J.D., 2006. Treatment of landfill leachate by the Fenton process. Water Res. 40, 3683–3694.

Duong, L.V., Wood, B.J., Kloprogge, J.T., 2005. XPS study of basic aluminum sulphate and basic aluminium nitrate. Mater. Lett. 59, 1932–1936.
Elkins, K.M., Nelson, D.J., 2002. Spectroscopic approaches to the study of the interaction of aluminum with humic substances. Coord. Chem. Rev. 228, 205–225.
Ernst, M., Lurot, F., Schrotter, J.-C., 2004. Catalytic ozonation of refractory organic model compounds in aqueous solution by aluminum oxide. Appl. Catal. B Environ. 47, 15–25.
Farvardin, M.R., Collins, A.G., 1989. Preozonation as an aid in the coagulation of humic substances—optimum preozonation dose. Water Res. 23, 307–316.
Fotiou, T., Triantis, T.M., Kaloudis, T., Papaconstantinou, E., Hiskia, A., 2014. Photocatalytic degradation of water taste and odour compounds in the presence of polyoxometalates and TiO2: intermediates and degradation pathways. J. Photochem. Photobiol. Chem. 286, 1–9.
Francioso, O., Sánchez-Cortés, S., Casarini, D., Garcia-Ramos, J.V., Ciavatta, C., Gessa, C., 2002. Spectroscopic study of humic acids fractionated by means of tangential ultrafiltration. J Mol Struc-Theochem 609, 137–147.
Haag, W.R., Yao, C.C.D., 1992. Rate constants for reaction of hydroxyl radicals with several drinking water contaminants. Environ. Sci. Technol. 26, 1005–1013.
Han, X., Lu, H., Gao, Y., Chen, X., Yang, M., 2020. The role of in situ Fenton coagulation on the removal of benzoic acid. Chemosphere 238, 124632.
Hiradate, S., Yamaguchi, N.U., 2003. Chemical species of Al reacting with soil humic acids. J. Inorg. Nucl. Chem. 97, 26–31.
Huang, Y., Luo, M., Xu, Z., Zhang, D., Li, L., 2019. Catalytic ozonation of organic contaminants in petrochemical wastewater with iron-nickel foam as catalyst. Separ. Purif. Technol. 211, 269–278.
Hübner, U., von Gunten, U., Jekel, M., 2015. Evaluation of the persistence of transformation products from ozonation of trace organic compounds–A critical review. Water Res. 68, 150–170.
Iglesias, A., López, R., Fiol, S., Antelo, J.M., Arce, F., 2003. Analysis of copper and calcium–fulvic acid complexation and competition effects. Water Res. 37, 3749–3755.
Ikhlaq, A., Brown, D.R., Kasprzyk-Hordern, B., 2012. Mechanisms of catalytic ozonation on alumina and zeolites in water: formation of hydroxyl radicals. Appl. Catal. B Environ. 123, 94–106.
Italiano, C., Luchters, N., Pino, L., Fletcher, J., Specchia, S., Fletcher, J., Vita, A., 2018. High specific surface area supports for highly active Rh catalysts: syngas production from methane at high space velocity. Int. J. Hydrogen Energy 43, 11755–11765.
Jin, P., Jin, X., Bjerkelund, V.A., Østerhus, S.W., Wang, X.C., Yang, L., 2016. A study on the reactivity characteristics of dissolved effluent organic matter (EfOM) from municipal wastewater treatment plant during ozonation. Water Res. 88, 643–652.
Jin, P., Jin, X., Wang, X.C., Shi, X., 2013. An analysis of the chemical safety of secondary effluent for reuse purposes and the requirement for advanced treatment. Chemosphere 91, 558–562.
Jin, P., Song, J., Yang, L., Jin, X., Wang, X.C., 2018. Selective binding behavior of humic acid removal by aluminum coagulation. Environ. Pollut. 233, 290–298.
Jin, X., Jin, P., Hou, R., Yang, L., Wang, X.C., 2017. Enhanced WWTP effluent organic matter removal in hybrid ozonation-coagulation (HOC) process catalyzed by Al-based coagulant. J. Hazard Mater. 327, 216–224.
Jin, X., Liu, Y., Wang, Y., Zhang, S., Zhang, W., Jin, P., Xu, L., Shi, X., Wang, X.C., Lv, S., 2020a. Towards a comparison between the hybrid ozonation-coagulation (HOC) process using Al- and Fe-based coagulants: performance and mechanism. Chemosphere 253, 126625.
Jin, X., Shi, Y., Hou, R., Zhang, W., Jin, P., Wang, X., 2019a. Role of Al-based coagulants on a hybrid ozonation–coagulation (HOC) process for WWTP effluent organic matter and ibuprofen removal. Environ Sci-Wat Res 5, 599–608.
Jin, X., Wang, Y., Zhang, W., Jin, P., Wang, X.C., Wen, L., 2019b. Mechanism of the hybrid ozonation-coagulation (HOC) process: comparison of preformed Al13 polymer and in situ formed Al species. Chemosphere 229, 262–272.
Jin, X., Xie, X., Liu, Y., Wang, Y., Wang, R., Jin, P., Yang, C., Shi, X., Wang, X.C., Xu, H., 2020b. The role of synergistic effects between ozone and coagulants (SOC) in the electro-hybrid ozonation-coagulation process. Water Res. 177, 115800.
Kim, H.-C., Yu, M.-J., 2005. Characterization of natural organic matter in conventional water treatment processes for selection of treatment processes focused on DBPs control. Water Res. 39, 4779–4789.
Kögel-Knabner, I., 1997. 13C and 15N NMR spectroscopy as a tool in soil organic matter studies. Geoderma 80, 243–270.
Kölbl, A., Kögel-Knabner, I., 2004. Content and composition of free and occluded particulate organic matter in a differently textured arable Cambisol as revealed by solid-state 13C NMR spectroscopy. J. Plant Nutr. Soil Sci. 167, 45–53.
Kostic, I., Andjelkovic, T., Nikolic, R., Bojic, A., Purenovic, M., Blagojevic, S., Andjelkovic, D., 2011. Copper(II) and lead(II) complexation by humic acid and humic-like ligands. J. Serb. Chem. Soc. 76, 1325–1336.
Li, F., Zhang, L., Evans, D.G., Duan, X., 2004. Structure and surface chemistry of manganese-doped copper-based mixed metal oxides derived from layered double hydroxides. Colloid. Surface. Physicochem. Eng. Aspect. 244, 169–177.
Li, T., Yan, X., Wang, D., Wang, F., 2009. Impact of preozonation on the performance of coagulated flocs. Chemosphere 75, 187–192.
Lin, J.-L., Huang, C., Dempsey, B., Hu, J.-Y., 2014. Fate of hydrolyzed Al species in humic acid coagulation. Water Res. 56, 314–324.
Lin, J.-L., Huang, C., Pan, J.R., Wang, D., 2008. Effect of Al(III) speciation on coagulation of highly turbid water. Chemosphere 72, 189–196.
Liu, H., Hu, C., Zhao, H., Qu, J., 2009. Coagulation of humic acid by PACl with high content of Al13: the role of aluminum speciation. Separ. Purif. Technol. 70, 225–230.
Luo, Y., Guo, W., Ngo, H.H., Nghiem, L.D., Hai, F.I., Zhang, J., Liang, S., Wang, X.C., 2014. A review on the occurrence of micropollutants in the aquatic environment and their fate and removal during wastewater treatment. Sci. Total Environ. 473–474, 619–641.
Mao, J., Olk, D.C., Fang, X., He, Z., Schmidt-Rohr, K., 2008. Influence of animal manure application on the chemical structures of soil organic matter as investigated by advanced solid-state NMR and FT-IR spectroscopy. Geoderma 146, 353–362.
Meunier, L., Canonica, S., von Gunten, U., 2006. Implications of sequential use of UV and ozone for drinking water quality. Water Res. 40, 1864–1876.
Miikki, V., Senesi, N., Hänninen, K., 1997. Characterization of humic material formed by composting of domestic and industrial biowastes: Part 2 spectroscopic evaluation of humic acid structures. Chemosphere 34, 1639–1651.
Monteil-Rivera, F., Brouwer, E.B., Masset, S., Deslandes, Y., Dumonceau, J., 2000. Combination of X-ray photoelectron and solid-state 13C nuclear magnetic resonance spectroscopy in the structural characterisation of humic acids. Anal. Chim. Acta 424, 243–255.
Nawrocki, J., Kasprzyk-Hordern, B., 2010. The efficiency and mechanisms of catalytic ozonation. Appl. Catal. B Environ. 99, 27–42.
Oliver, B.G., Thurman, E.M., Malcolm, R.L., 1983. The contribution of humic substances to the acidity of colored natural waters. Geochem. Cosmochim. Acta 47, 2031–2035.
Önnby, L., Walpen, N., Salhi, E., Sander, M., von Gunten, U., 2018. Two analytical approaches quantifying the electron donating capacities of dissolved organic matter to monitor its oxidation during chlorination and ozonation. Water Res. 144, 677–689.
Pei, Y., Yu, J., Guo, Z., Zhang, Y., Yang, M., Zhang, J., Junji, H., 2007. Pilot study on preozonation enhanced drinking water treatment process. Ozone Sci. Eng. 29, 317–323.
Pinheiro, J.P., Mota, A.M., Benedetti, M.F., 2000. Effect of aluminum competition on lead and cadmium binding to humic acids at variable ionic strength. Environ. Sci. Technol. 34, 5137–5143.
Provenzano, M.R., D'Orazio, V., Jerzykiewicz, M., Senesi, N., 2004. Fluorescence behaviour of Zn and Ni complexes of humic acids from different sources. Chemosphere 55, 885–892.
Qi, F., Xu, B., Chen, Z., Ma, J., Sun, D., Zhang, L., 2009. Efficiency and products investigations on the ozonation of 2-methylisoborneol in drinking water. Water Environ. Res. 81, 2411–2419.
Reckhow, D.A., Legube, B., Singer, P.C., 1986. The ozonation of organic halide precursors: effect of bicarbonate. Water Res. 20, 987–998.
Sam, S., Yukselen, M., Zorba, M., Gregory, J., 2010. The effect of ozone on the reversibility of floc breakage: suspensions with high humic acid content. Ozone Sci. Eng. 32, 435–443.
Schnitzer, M., Khan, S.U., 1972. Humic substances in the environment. Soil Sci. Soc. Am. J. 39, 130.
Schulten, H.R., Schnitzer, M., 1993. A state of the art structural concept for humic substances. Naturwissenschaften 80, 29–30.
Sharpless, C.M., Mcgown, L.B., 1999. Effects of aluminum-induced aggregation on the fluorescence of humic substances. Environ. Sci. Technol. 33, 3264–3270.
Song, J., Jin, P., Jin, X., Wang, X.C., 2019a. Synergistic effects of various in situ hydrolyzed aluminum species for the removal of humic acid. Water Res. 148, 106–114.
Song, J., Jin, X., Wang, X.C., Jin, P., 2019b. Preferential binding properties of carboxyl and hydroxyl groups with aluminium salts for humic acid removal. Chemosphere 234, 478–487.
Stephenson, R.J., Duff, S.J.B., 1996. Coagulation and precipitation of a mechanical pulping effluent—I. Removal of carbon, colour and turbidity. Water Res. 30, 781–792.
Suresh, C., Santhanaraj, D., Gurulakshmi, M., Deepa, G., Shanthi, K., 2012. Mo-Ni/Al-SBA-15 (sulfide) catalysts for hydrodenitrogenation: effect of Si/Al ratio on catalytic activity. ACS Catal. 2, 127–134.
Tipping, E., 2005. Cation Binding by Humic Substances. Cambridge University Press.
Tipping, E., Backes, C.A., Hurley, M.A., 1988. The complexation of protons, aluminium and calcium by aquatic humic substances: a model incorporating binding-site heterogeneity and macroionic effects. Water Res. 22, 597–611.
Von Sonntag, C., Von Gunten, U., 2012. Chemistry of Ozone in Water and Wastewater Treatment. IWA publishing.
Walpen, N., Houska, J., Salhi, E., Sander, M., von Gunten, U., 2020. Quantification of the electron donating capacity and UV absorbance of dissolved organic matter during ozonation of secondary wastewater effluent by an assay and an automated analyzer. Water Res. 185, 116235.
Wang, B., Zhang, Y., Qin, Y., Li, H., 2021. Removal of Microcystis aeruginosa and control of algal organic matter by Fe(II)/peroxymonosulfate pre-oxidation enhanced coagulation. Chem. Eng. J. 403, 126381.
Wang, J., Chen, H., 2020. Surface hydroxyl groups of synthetic α-FeOOH in promoting •OH generation from aqueous ozone: property and activity relationship. Sci. Total Environ. 704, 135241–135249.
Westerhoff, P., Aiken, G., Amy, G., 1999. Relationships between the structure of natural organic matter and its reactivity towards molecular ozone and hydroxyl radicals. Water Res. 33, 2265–2276.
White, D.M., Garland, D.S., Narr, J., Woolard, C.R., 2003. Natural organic matter and DBP formation potential in Alaskan water supplies. Water Res. 37, 939–947.
Wu, Y., Zhou, S., Qin, F., Peng, H., Lai, Y., Lin, Y., 2010. Removal of humic substances

from landfill leachate by Fenton oxidation and coagulation. Process Saf Environ 88, 276–284.
Wu, Y., Zhou, S., Ye, X., Zhao, R., Chen, D., 2011. Oxidation and coagulation removal of humic acid using Fenton process. Colloid. Surface. 379, 151–156.
Xiaoli, C., Shimaoka, T., Qiang, G., Youcai, Z., 2008. Characterization of humic and fulvic acids extracted from landfill by elemental composition, 13C CP/MAS NMR and TMAH-Py-GC/MS. Waste Manag. 28, 896–903.
Xie, P., Chen, Y., Ma, J., Zhang, X., Zou, J., Wang, Z., 2016. A mini review of preoxidation to improve coagulation. Chemosphere 155, 550–563.
Yan, M., Wang, D., Shi, B., Wang, M., Yan, Y., 2007. Effect of pre-ozonation on optimized coagulation of a typical north-China source water. Chemosphere 69, 1695–1702.
Yan, Y., Gao, Y., Zheng, H., Yuan, B., Zhang, Q., Gu, Y., Zhuang, G., Wei, Z., Yao, Z., Zhong, X., Li, X., Wang, J., 2020. Simultaneous electrochemical ozone production and hydrogen evolution by using tantalum-based nanorods electrocatalysts. Appl. Catal. B Environ. 266, 118632.
Zhang, T., Li, C., Ma, J., Tian, H., Qiang, Z., 2008. Surface hydroxyl groups of synthetic α-FeOOH in promoting OH generation from aqueous ozone: property and activity relationship. Appl. Catal. B Environ. 82, 131–137.
Zhang, T., Ma, J., 2008. Catalytic ozonation of trace nitrobenzene in water with synthetic goethite. J. Mol. Catal. Chem. 279, 82–89.
Zhang, X., Yang, Z., Wang, Y., Gao, B.-Y., Yue, Q., 2012. The removal efficiency and reaction mechanism of aluminum coagulant on organic functional groups-carboxyl and hydroxyl. Chem. Eng. J. 211–212, 186–194.
Zhao, L., Sun, Z., Ma, J., 2009. Novel relationship between hydroxyl radical initiation and surface group of ceramic honeycomb supported metals for the catalytic ozonation of nitrobenzene in aqueous solution. Environ. Sci. Technol. 43, 4157–4163.